Dual Nano-Carriers using Polylactide-block-Poly(N-isopropylacrylamide-random-acrylic acid) Polymerized from Reduced Graphene Oxide Surface for Doxorubicin Delivery Applications

Leila Khanizadeh[1], Raana Sarvari[,2,3], Bakhshali Massoumi[1], Samira Agbolaghi[4], Younes Beygi-Khosrowshahi[4]*

[1]Department of Chemistry, Payame Noor University, Tehran, Iran.
[2]Stem Cell Research Center, Tabriz University of Medical Sciences, Tabriz, Iran.
[3]Stem Cell And Regenerative Medicine Institute, Tabriz University of Medical Sciences, Tabriz, Iran.
[4]Chemical Engineering Department, Faculty of Engineering, Azarbaijan Shahid Madani University, Tabriz, Iran.

ABSTRACT

The stimuli-responsive nanocomposites were designed as drug delivery nanocarriers. Thanks to promising properties such as large surface area and easy chemical functionalization, the graphene derivatives can be used for the drug delivery applications. For this purpose, in the current work, the poly(L,D-lactide)-*block*-poly(*N*-isopropylacrylamide-*rand*-acrylic acid) grafted from reduced graphene oxide (rGO-*graft*-PDLA-*block*-P(NIPAAm-*rand*-AAc)) was synthesized by the ring opening polymerization (ROP) and atom transfer radical polymerization (ATRP). As compared with the traditional radical polymerizations, living polymerizations are among the most-utilized methods to achieve surface initiated polymer brushes as they provide excellent control over the polymers composition. The average sizes of rGO-*graft*-PDLA-*block*-P(NIPAAm-*rand*-AAc) nanocomposite using the dynamic light scattering (DLS) measurements at pH values of 4.0 and 7.4 were 240 and 150 nm, respectively. The lower critical solution temperature (LCST) of rGO-*graft*-PDLA-*block*-P(NIPAAm-*rand*-AAc) was determined to be 39 °C through the ultraviolet-visible (UV-Vis) spectroscopy. The doxorubicin hydrochloride (DOX)-loading capacity was 99 %. The release of DOX increased at 42 °C compared to 37 °C. The results confirmed that the pH- and temperature-dependent releasing of this drug nano-carrier was beneficial for the anticancer at the tumor-like environment. The biocompatibility was also confirmed by assessing the survival rate of breast cancer cell line (MCF7) using 3-(4,5-dimethylthiazol-2-yl)-2,5-diphenyltetrazolium bromide (MTT) assay. The synthesized nanoparticles would have an excellent potential in the anticancer drug delivery.

Keywords: rGO; NIPAAm; PDLA; graft polymerization; drug delivery; stimuli-responsivity.

1. Introduction

Recently, stimuli-responsive smart nanomaterials have been synthesized for the ranostric applications, such as cellular imaging, drug delivery, and tumor therapy [1,2]. In particular, thermal- and pH-responsive polymers have been employed for biological applications [3]. Poly(*N*-isopropylacrylamide) (PNIPAAm), one of the thermo-responsive smart polymers, possesses excellent characteristics such as lower critical solution temperature (LCST) and phase transition. The PNIPAAm is generally hydrophilic below LCST, whereas it undergoes phase transition into hydrophobic above LCST [4,5]. The hydrophilic

monomers enable the increase of LCST in PNIPAAm [6]. The formation of polymer nanocomposites of different hydrophilicity and thus LCST are possible by varying monomer ratios [7]. The hydrophilic PNIPAAm becomes hydrophobic in hyperthermic tumor tissues, indicating high efficacy of cellular uptake and controlled drug release. Given this thermo-responsive property, the PNIPAAm is of great potential for tumor targeting and therapy applications [6]. On the other hand, pH-responsive polymers contain weak acids and bases functional groups such as carboxylic acids, phosphoric acid, and amines, exhibiting a change in the ionization state upon pH change, accompanying reversible variance activity in volume, solubility, and equipoise between the extended and collapsed state [8,9]. By regarding these facts, more efforts have been devoted to design the multifunctional materials based on the biocompatible polymers as drug delivery nano-systems. The application of these nano-systems reflected improved therapeutic results with less side effects through minimizing the drug degradation and increasing the availability of the drug at the disease site [10−15].

Graphene is one of the carbon-based materials with great scientific interest owing to its charming features that could be useful for a variety of applications. Thanks to excellent charge carrier mobility [16], promising electrical [17] and mechanical [18] properties and also high transparency [19], graphene can be used for the electronic components, energy storage, sensing and drug delivery [20−24]. In particular, graphene is of great potential for drug delivery applications due to large surface area and easy chemical functionalization [6,25]. Different from graphene, graphene oxide (GO) is hydrophilic and has abundant oxygen-containing functional groups and residual C=C double bonds, thereby can be grafted with the PNIPAAm chains through both covalent and non-covalent interactions [26,27]. The atom transfer radical polymerization (ATRP) is a well-known useful approach for an efficient modification of GO nanosheets. Some researchers demonstrated the effectiveness of the ATRP strategy to synthesize styrene, methylmethacrylate, and butylacrylate, etc. from the surface of GO [28−31]. As compared with the traditional radical polymerizations, ATRP is among the most-utilized methods to achieve surface initiated polymer brushes as they provide excellent control over the polymers composition [32,33]. By considering Doxorubicin hydrochloride

(DOX) as a drug model, the strong interaction of DOX with the pH-responsive blocks and the pH-sensitive drug release from polymer make the system very useful as a controlled drug delivery system [34,35].

Herein, we report the preparation of materials that combine the unique features of graphene, thermo-responsive poly(N-isoprppylacrylamide), and pH-responsive poly(acrylic acid) (PAA), resulting in a thermo- and pH-tunable dispersion of graphene nanosheets in aqueous solution. In this regard, L,D-lactide monomer was polymerized from –OH groups of reduced graphene oxide (rGO) and in the next step, ATRP initiator was attached onto –OH groups and converted to the ATRP agent. Subsequently, poly(L,D-lactide)-*block*-poly(*N*-isopropylacrylamide-*random*-acrylic acid) grafted from rGO (rGO-*g*-PDLA-*b*-P(NIPAAm-*rand*-AAc)) nanocomposite was reached through random copolymerization of NIPAAm and AAc monomers. Fourier transform infrared spectroscopy (FT-IR), thermogravimetric analysis (TGA), X-ray diffraction (XRD), and field emission scanning electron microscopy (FESEM) were utilized to characterize the structure of different nanostructures. Furthermore, the solution stability of the nanosheets and their pH- and thermo-responsibility were measured by dynamic light scattering (DLS) and ultraviolet-visible (UV-Vis) spectroscopy.

2. Experimental
2.1. Materials

Graphite, potassium permanganate ($KMnO_4$), sodium nitrate ($NaNO_3$), hydrochloric acid (HCl), sulfuric acid (H_2SO_4) and sodium bore hydride ($NaBH_4$) were purchased from Merck (Darmstadt, Germany) and used as received. Acetic acid was distilled under reduced pressure and then stored at –15 °C prior to use. The NIPAAm (97%, Sigma-Aldrich, USA) was purified using recrystallization from *n*-hexane/toluene mixture. Copper (I) bromide (CuBr) was purchased from Sigma-Aldrich and was purified by stirring in acetic acid three times, then washed with ethanol and dried under vacuum. 2-Bromoisobutyrylbromide (BIBB) and N,N,N',N'',N''-pentamethyldiethylenetriamine (PMDETA) were purchased from Merck Chemicals. DOX was prepared from Exir Nano Sina Company (Iran). The D,L-lactide and stannous(II)2-ethylhexanoate ($Sn(Oct)_2$) were prepared from Sigma-Aldrich (USA). 2-Hydroxyethyl

methacrylate (Merck, Darmstadt, Germany) was dried over calcium hydride, vacuum-distilled, and then stored at −20 °C prior to use. All other reagents were purchased from Merck and purified according to the standard methods.
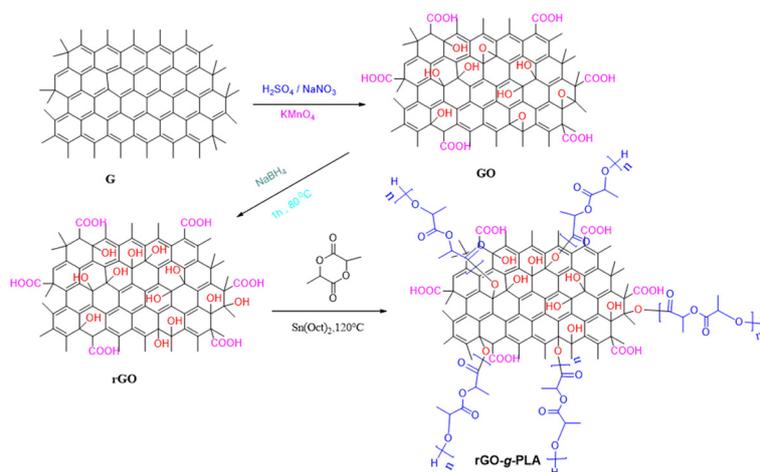
2.2. Synthesis of rGO grafted with poly(L,D-lactide) (rGO-*g*-PDLA)

First, rGO was prepared according to the literature (Scheme1) [36]. The chemical grafting of PDLA onto the rGO nanosheets was carried out by the grafting-from approach based on in situ ring opening polymerization of L,D-lactide [35]. In a typical experiment, rGO and L,D-lactide monomer were added into a Schleich tube to form dispersion solution under sonication at room temperature for 1 h and then, tin(II) 2-ethylhexanoate and Sn(Oct)$_2$ were added into the reaction tube. The reaction was performed under pure argon within 24 h at 120 °C.
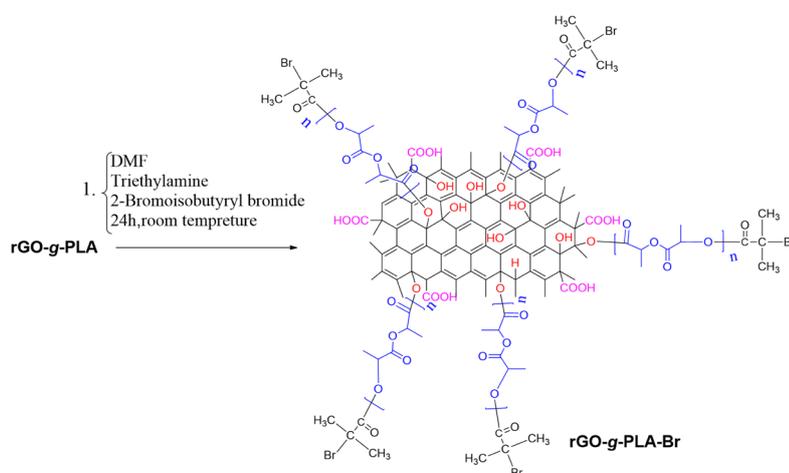
After the desired time, a homogeneous black solid (rGO-*g*-PDLA) was obtained. The original solid was then dissolved in tetrahydrofuran (THF) and precipitated in cold methanol (Scheme1).

2.3. Synthesis of rGO-*g*-PDLA-Br macroinitiator

The rGO-*g*-PDLA was treated with ATRP initiator of α-bromoisobutyryl bromide to form rGO-*g*-PDLA-Br (Scheme 2). In details, a 100 mL reactor containing rGO-*g*-PDLA (0.50 g), anhydrous dimethylformamide (DMF) (10.0 mL), and triethylamine (0.30 g, 1.67 mmol) was evacuated and filled with high pure argon. Then, 0.38 g (1.67 mmol) of α-bromoisobutyryl bromide was dissolved in 5 mL anhydrous DMF and added to the reaction dropwise at 0 °C for 60 min. The resulting mixture was stirred for 3 h at 0 °C and then at room temperature for 48 h. The solid was then separated from the mixture by centrifugation

Scheme 1- Synthesis of rGO-*g*-PDLA.

Scheme 2- Synthesis of rGO-*g*-PDLA-Br.

and washed with an excessive amount of distilled water to remove the salts formed during the reaction. The raw product was dispersed in 20 mL of DMF, centrifugation and washed thrice with DMF and acetone. The solid was collected and dried overnight under vacuum at 40 °C.

2.4. Synthesis of rGO-*g*-PDLA-*block*-P(NIPAAm-*rand*-AAc)

In situ polymerization of NIPAAm and AAc in the presence of rGO-*g*-PDLA via ATRP afforded rGO-*g*-PDLA-Br. In more details, 30.0 mg rGO-*g*-PDLA-Br, 7.2 mg (0.05 mmol) CuBr, 8.7 mg (0.05 mmol) N,N,N',N",N"-pentamethyldiethylenetriamine (PMDETA), and DMF/H$_2$O (30/30 mL) were placed in a 10 mL reactor, which was then sealed with a rubber plug. The reactor was evacuated and filled thrice with argon. 25.0 mg (0.24 mmol) of NIPAAm and 5.76 mg (0.08 mmol) acrylic acid (AA) were injected into the reactor. The reactor was then immersed in an oil bath at 65 °C and its contents were stirred for 24 h. The mixture was subsequently diluted with DMF and rGO-*g*-PDLA-*b*-P(NIPAAm-*rand*-AAc) was obtained by centrifugation. The filter product was redispersed in DMF by sonication and precipitated in distilled water to remove the Cu/PMDETA complex and unreacted monomer. The product was then dried overnight under vacuum (Scheme 3).

2.5. Preparation of Doxorubicin hydrochloride (DOX)-loaded rGO-*g*-PDLA-*b*-P(NIPAAm-*rand*-AAc)

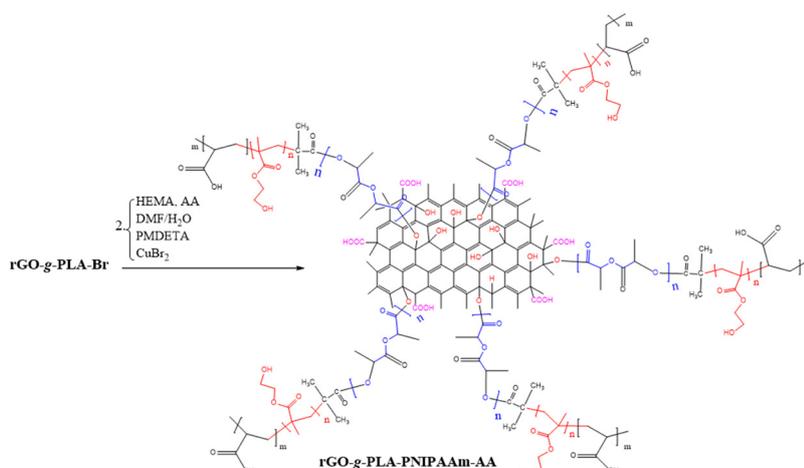The rGO-*g*-PDLA-*b*-P(NIPAAm-*rand*-AAc) (150 mg) and DOX (20 mg) were dissolved in deionized water (10 mL) under stirring at room temperature. The content of flask was sonicated for 15 min and then stirred for about 48 h in the dark at room temperature to reach the maximum loading content. The DOX-loaded nano-carriers were collected by centrifugation at 7000 rpm for 15 min. The DOX-encapsulation efficiency was determined by UV-Vis spectroscopy at 472 nm and calculated using Equation (1) [15].

$$EE(\%) = \frac{(C_T - C_{DOX})}{C_T} \times 100 \qquad (1)$$

where C$_T$ is total DOX concentration for loading, and C$_{DOX}$ is DOX concentration in filtrate solution. The DOX-encapsulation efficiency was calculated to be 99.1%.

2.6. Evaluation of *in vitro* pH- and temperature-dependent release of DOX

In the *in vitro* drug release experiment, DOX-loaded nano-carrier (60 mg) was suspended in phosphate buffered saline (PBS) with different pH values (7.4, 5.4, and 4), sealed in a dialysis membrane bag with a molecular cut off of 1 kDa and placed in PBS (0.01 mol L^{-1}, 100 mL). The release solution was stirred at 200 rpm individually at 37 and 42 °C, and then 2 mL of buffer solution was collected in different times to investigate with UV-Vis spectrophotometer at 480 nm. The percentage of cumulative amount of released DOX was calculated from the standard calibration curve. The purpose of drug release at various pH values was to demonstrate that the release was higher at acidic pHs and the nano-carrier was pH-sensitive; because the cancer cells are acidic and the pH-sensitive nano-carrier could be effective for smart drug releasing in cancer areas without damaging the normal cells.

Scheme 3- Synthesis of rGO-*g*-PDLA-*b*-P(NIPAAm-*rand*-AAc).

2.7. Characterization

Fourier transform infrared (FT-IR) spectra of the samples were recorded on a Shimadzu 8101M FT-IR (Shimadzu, Kyoto, Japan) between the wavenumbers of 4000–400 cm^{-1}. The samples were prepared by grinding the dry powders with potassium bromide (KBr) and compressing the mixture into disks. The thermal gravimetric analysis (TGA) experiments were conducted under nitrogen atmosphere at a temperature range of 25–700 °C with heating rate of 10 °C min^{-1}. The ultraviolet-visible (UV-Vis) spectroscopy was performed using a Shimadzu 1650 PC UV-Vis spectrophotometer (Shimadzu, Kyoto, Japan) at the wavelength range of 250–1000 nm. The field emission scanning electron microscope (FESEM) type 1430 VP (LEO Electron Microscopy Ltd, Cambridge, UK) was used to characterize the surface morphology of synthesized samples. The X-ray diffraction (XRD) spectra were obtained with a Siemens D 5000 (Aubrey, Texas, USA), X-ray generator (CuKα radiation with λ=1.5406 Å) with a 2θ scan range of 15 to 70° at room temperature. Dynamic light scattering (DLS) measurements were conducted using zeta plus (Brookhaven, USA) at room temperature. The samples were prepared as 0.5 mg per mL in distilled deionized water with adjusting the solution pH by adding HCl or NaOH.

3. Results and Discussion

3.1. Characterization of rGO-*g*-PDLA-*b*-P(NIPAAm-*rand*-AAc)

3.1.1. FT-IR spectra

The rGO-*g*-PDLA was synthesized by a ROP approach and the hydroxyl end groups in PDLA were further reacted with α-bromoisobutyrylbromide to reach the functionalized rGO-*g*-PDLA nanosheets as initiator. FT-IR spectra of rGO, rGO-*g*-PDLA, and rGO-*g*-PDLA-Br are displayed in Fig. 1. FT-IR spectrum of rGO represented the stretching vibrations of aliphatic and aromatic C–H at 2800–3100 cm^{-1} and –OH stretching vibration at 3400 cm^{-1}. Furthermore, the intensity of the hydroxyl stretching vibration significantly increased and most of the carbonyl and epoxy groups were removed. In FT-IR spectra of rGO-*g*-PDLA, the stretching vibration of carbonyl group was detected at 1733 cm^{-1} and the intensity of the hydroxyl stretching vibration also decreased. This verified the synthesis of rGO-*g*-PDLA. After addition of ATRP reagent, the disappearance of –OH groups due to PDLA and appearance of stretching vibration at

682 cm^{-1} for Br proved the synthesis of rGO-*g*-PDLA-Br. FT-IR spectra of PNIPAAm can be listed as: aliphatic C–H stretching vibrations at 2800–2950 cm^{-1}, stretching vibration of carbonyl group at 1772 cm^{-1}, C–H bending vibration at 1411 cm^{-1}, stretching vibration of C–O group at 1325 cm^{-1} and C–O–C stretching vibration at 1166 cm^{-1}. The main absorption bands in P(NIPAAm-*rand*-AAc) copolymers demonstrated the stretching vibrations of carbonyl groups of PNIPAAm and PAAc at 1778 and 1691 cm^{-1}, respectively. The absorption bands of –NH secondary amid and –OH group of –COOH in polyacrilic acid were overlapped at 3400–3520 cm^{-1}.

3.1.2. Thermogravimetric analyses (TGA)

As represented in Fig. 2, the rGO was thermally unstable and some mass losses were detected around 150 °C for the presence of water molecules. It also showed a sharp weight loss of 30% between 150 and 700 °C, which was ascribed to the pyrolysis or decomposition of oxygen functional groups such as hydroxyl, carboxylic acid, and epoxide groups [37]. However, there were two clearly separated weight loss stages in the range of 140 °C and 140–450 °C for GO-g-PDLA, assigning to the loss of oxygen-containing functional groups on
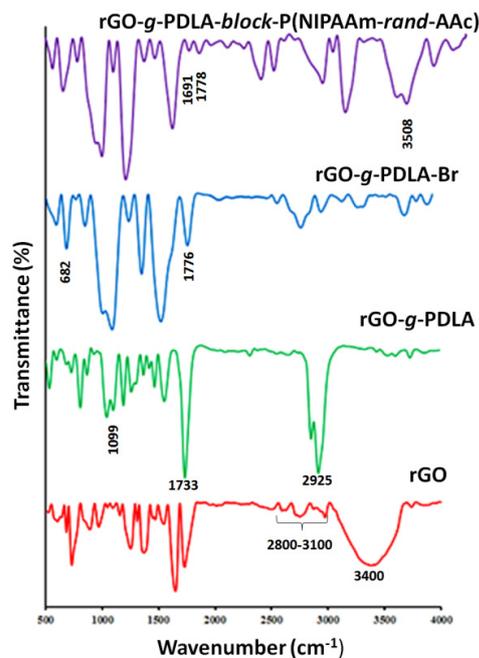

Fig. 1- FT-IR spectra of rGO, rGO-*g*-PDLA, rGO-*g*-PDLA-Br and rGO-*g*-PDLA-*b*-P(NIPAAm-*rand*-AAc).
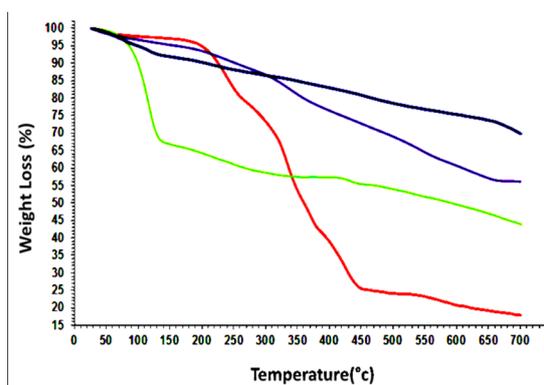
Fig. 2- TGA curves of rGO (blue), rGO-PDLA (purple), rGO-PDLA-Br (green) and rGO-*g*-PDLA-*b*-P(NIPAAm-*rand*-AAc) (red).

Fig. 3- XRD patterns of rGO (a), rGO-PDLA (b), and rGO-*g*-PDLA-*b*-P(NIPAAm-*rand*-AAc) (c).

rGO and grafted PDLA chains [38,39], respectively. The weight loss of GO-*g*-PDLA continued after 450 °C (Fig. 2). However, PDLA was decomposed completely before 450 °C, as seen in Fig. 2 [40,41]. Therefore, the content of PDLA grafted to rGO was about 20 wt%, corresponding to the weight loss of the degradation of PDLA. The small weight loss of rGO-*g*-PDLA after 450 °C might be caused by the decomposition of the treated rGO [42] or other impurities. The rGO-g-PDLA-Br initiator exhibited a continuous weight loss until 700 °C thanks to the cleavage of the initiator moiety, followed by further weight loss up to about 38% because of the decomposition of rGO, PDLA, and initiator moiety. After ATRP polymerization of NIPAAm and AAc, rGO-*g*-PDLA-*b*-P(NIPAAm-*rand*-AAc) sample represented a relatively large mass loss of 80% between 230–450 °C, correlating with the decomposition of PDLA, PNIPAAm, and PAAc chains grafted onto the nanosheets. The mass loss increased to 80 wt% after copolymerization of NIPAAm and AAc. which proved that the pH-sensitive block was added to the polymer chains successfully [43].

3.1.3. X-Ray diffraction study

The XRD patterns for rGO, rGO-PDLA, and rGO-*g*-PDLA-*b*-P(NIPAAm-*rand*-AAc) nanosheets are represented in Fig. 3. The broad amorphous peak at 2θ = 24° was assigned to rGO (Fig. 3(a)). The peaks appeared at 2θ = 14.2, 17.5, and 22° were related to the ordering of PDLA segments, which were not very sharp and intensified (Fig. 3(b)). The peak of 24° was for rGO. In Fig. 3(c), the peaks of
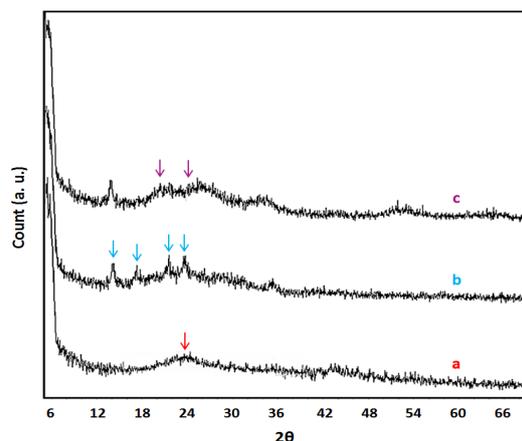
20 and 25° were assigned to PNIPAAm and rGO, respectively. The broad peaks at the higher 2θ values were also detected for the presence of PNIPAAm and PAAc grafts.

3.1.4. Morphology study

Figs. 4(a-d) show FESEM images of rGO, rGO-PDLA, rGO-PDLA-Br and rGO-*g*-PDLA-*b*-P(NIPAAm-*rand*-AAc) samples, respectively. The rGO nanosheets were wrinkled with a typical lamella structure (Fig. 4(a)). As represented in Fig. 4(b), the surface of rGO nanosheets became rougher after polymerization of PDLA onto them. In addition, the morphologies of rGO-PDLA-Br (Fig. 4(c)) and rGO-*g*-PDLA-*b*-P(NIPAAm-*rand*-AAc) (Fig. 4(d)) were different because of functionalization and further polymerization.

3.1.5. DLS measurements

The pH-response of rGO-*g*-PDLA-*b*-P(NIPAAm-*rand*-AAc) nanostructures was investigated by DLS measurements. The carboxylic acids on acrylic acid and amides on PNIPAAm could form hydrogen bonding [35,44]. At pH = 4, the diameters of micelles were approximately 687 nm. The size of these aggregates decreased to 256 nm at pH of 7.4 (25 °C). At a lower pH value, the hydrogen bonding occurred between PAAc and PNIPAAm. By increasing the pH, the disappearance of the hydrogen bonding occurred due to ionization of the carboxylic acid groups. DLS diagrams of rGO-*g*-PDLA-*b*-P(NIPAAm-*rand*-AAc) composite at various pH values are reported in Fig. 5 [45,46].
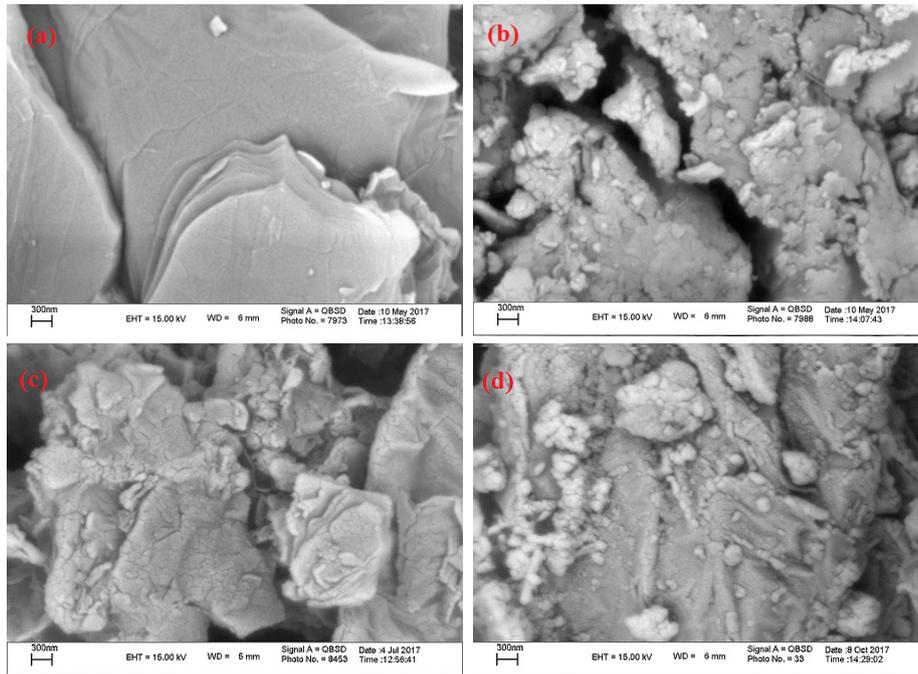
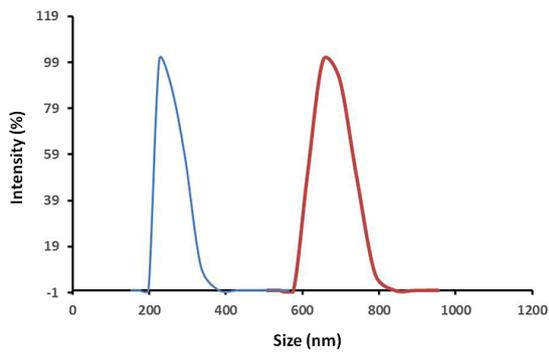Fig. 4- FESEM images of rGO (a), rGO-PDLA (b), rGO-PDLA-Br (c) and rGO-*g*-PDLA-*b*-P(NIPAAm-*rand*-AAc) (d).

Fig. 5- DLS diagrams of rGO-*g*-PDLA-*b*-P(NIPAAm-*rand*-AAc) composite at pH = 4 (red curve) and pH = 7.4 (blue curve).
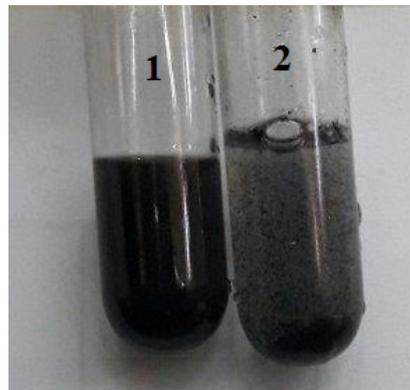

Fig. 6- Photograph of rGO-*g*-PDLA-*b*-P(NIPAAm-*rand*-AAc) at 25 °C (1) and at 39–40 °C.

3.1.6. LCST measurements

Thermo-responsive polymers usually exhibit a lower critical solution temperature (LCST) in water. Thermo-responsive polymers have been investigated in tissue engineering, drug delivery, and nanotechnology applications. The main reason is that the LCST of thermo-responsive polymers such as PNIPAAm is close to the body temperature (37 °C) [47,48]. All samples were solvated at 25 °C. As depicted in Fig. 6, by temperature elevation, the LCST of rGO-*g*-PDLA-*b*-P(NIPAAm-*rand*-AAc) sample ranged at 39–40 °C. Moreover, the

UV-Vis spectroscopy was employed for the LCST measurements. To this end, the transmittance of UV-Vis light was measured as a function of temperature. At low temperature, the samples were transparent and the light transmittance was high. However, by increasing the temperature, the polymer, especially PNIPAAm segments, commenced to aggregate and led to the phase separation. According to Fig. 7, the LCST of samples ranged at 39–40 °C, thereby the applied stimuli-responsive polymer was interesting in drug delivery for having a LCST behavior [35].

66

3.1.7. *In vitro* DOX release behavior

In vitro DOX release from composite-DOX was a pH- and temperature-responsive process, where the protonation of carboxyl groups in mildly acidic conditions resulted in a faster dissociation of composite-DOX complex, leading to increased release of DOX at low pH. The release of DOX from the composite was measured at 37 °C (below LCST) and 42 °C (above LCST). The release rate was different in buffer solution. Composite-DOX in buffer solution (37 °C) at pH of 7.4 was quite stable and delayed the release of loaded drug (Fig. 8(a). At the pH of 5.4 an accelerated release of DOX was detected. At lower pH (= 4), the protonation of polyacrylic acid block due to less repulsion

between adjacent carboxylic acid groups further accelerated the drug release. The release rates in buffer solution at 42 °C and at pHs of 4, 5.4 and 7.4 (Fig. 8(b)) were faster than those detected at 37 °C (Fig. 8(a)). It revealed that the release rates at 42 °C increased by the phase transition of hydrophilic at LCST, resulting in the disturbance of the composite core (Fig. 8(b)). According to Fig. 8(a), after 631 min the releases in pH values of 4, 5.4, and 7.4 were 38.2, 42.62, and 56.31%, respectively. By comparing with the standard of a burst release defined in the Chinese Pharmacopoeia (more than 40% of the drug being released in 0.5 h) [49], less than 20% of the drug was released from the nanocomposite during 1 h (9, 13, and 17% of DOX release within
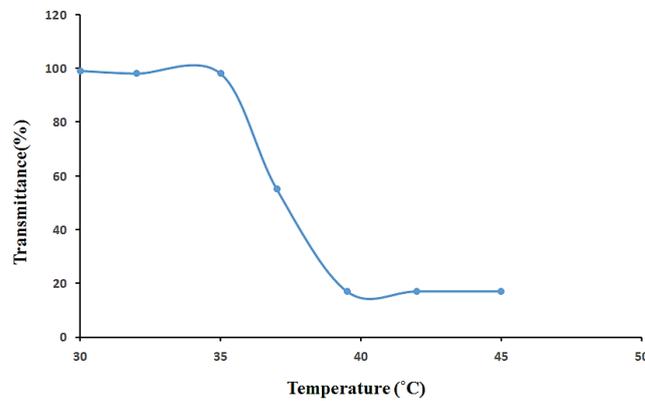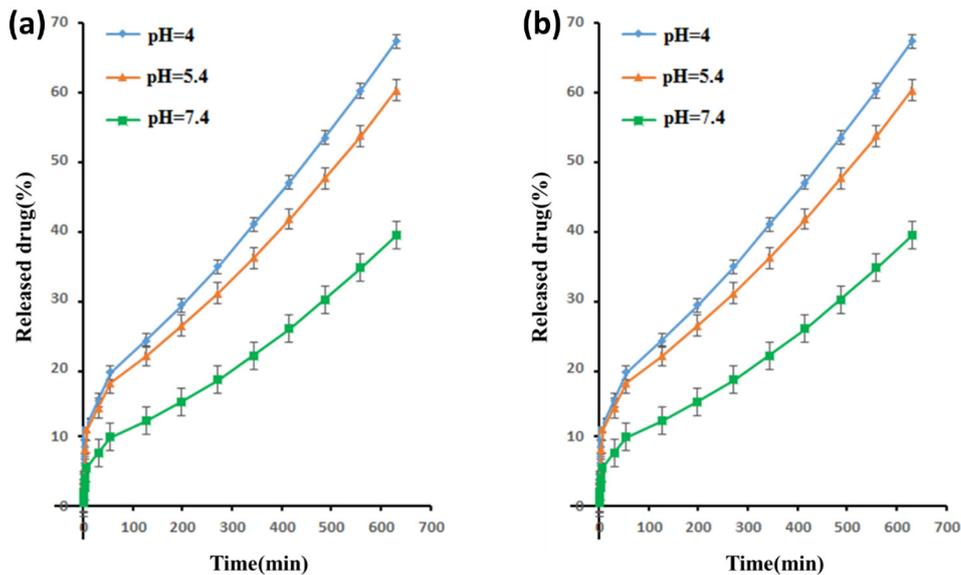

Fig. 7- LCST of rGO-*g*-PDLA-*b*-P(NIPAAm-*rand*-AAc).

Fig. 8- *In vitro* release profiles of DOX from rGO-*g*-PDLA-*b*-P(NIPAAm-*rand*-AAc) nanocomposite at various pHs at 37 °C (a) and 42 °C (b).

55 min), thereby it did not reach the burst release level. Less than 20% of DOX was released in physiological condition (pH 7.4 and 37 °C) during 1 h (first sampling time) (Fig. 8(a)). The thermo-responsive carrier under a structural transition as a response to increasing temperature leads to the certification of the drug and drug easier absorption by cells [50–52]. Hence, the release profiles at 42 °C in pH values of 4, 5.4 and 7.4 manifested that by elevating the temperature, the drug release values were accelerated to 39.05, 60.02, and 67.13%, respectively. This phenomenon may occur due to the collapse of the thermo-responsive segments (PNIPAM) at above LCST [52,53] of

nanocomposite owing to the compact loading of DOX in the nanocomposite [46].

3.1.8. *In vitro* cytotoxicity effect

The expansion factor and *in vitro* cytotoxicity are reported in Figs. 9 and 10, respectively. The expansion factors of rGO-*g*-PDLA-*b*-P(NIPAAm-*rand*-AAc)+DOX and rGO-*g*-PDLA-*b*-P(NIPAAm-*rand*-AAc)+cell were higher than DOX and MCF-7 cell line, respectively. *In vitro* cytotoxicity effects of the synthesized rGO-*g*-PDLA-*b*-P(NIPAAm-*rand*-AAc) nanocomposites and DOX-loaded rGO-*g*-PDLA-*b*-P(NIPAAm-*rand*-AAc) were studied using MTT assay against MCF-7 cells. The DOX-loaded
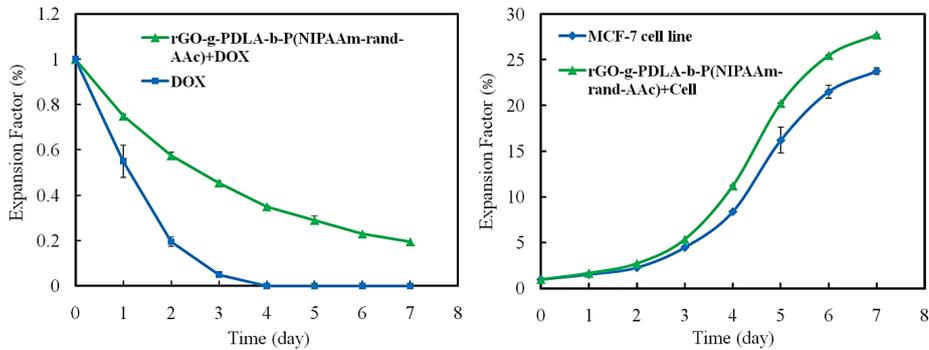

Fig. 9- Expansion factor of (a) DOX and rGO-*g*-PDLA-*b*-P(NIPAAm-*rand*-AAc)+DOX as well as (b) MCF-7 cell line and rGO-*g*-PDLA-*b*-P(NIPAAm-*rand*-AAc)+cell.
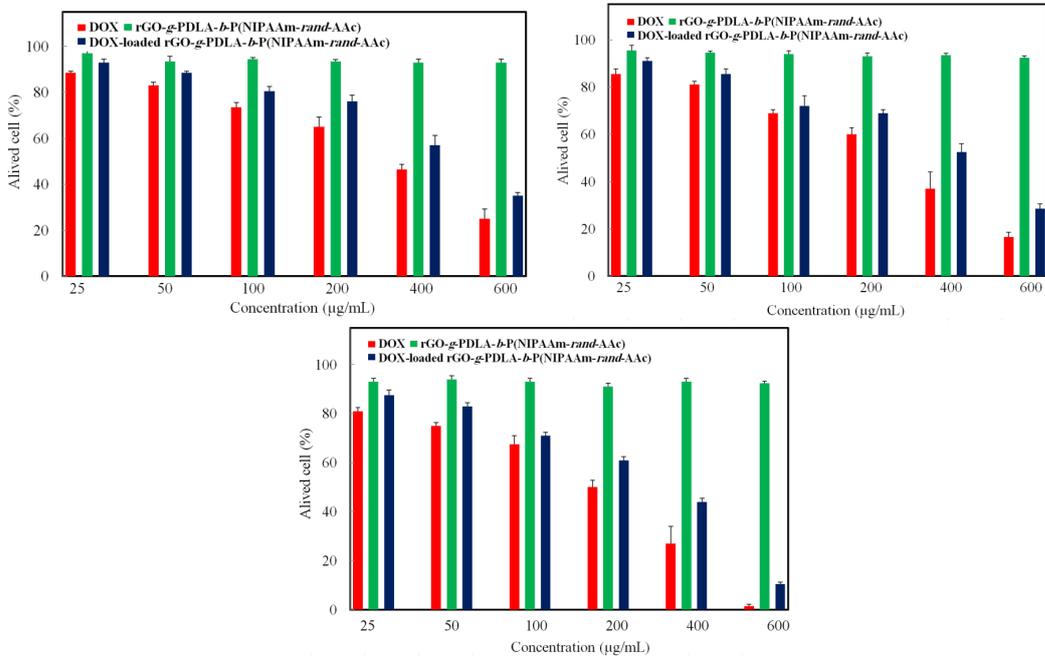

Fig. 10- Cytotoxicity assay results of rGO-*g*-PDLA-*b*-P(NIPAAm-*rand*-AAc) nanocomposites, DOX-loaded rGO-*g*-PDLA-*b*-P(NIPAAm-*rand*-AAc) and free DOX with different concentrations (25, 50, 100, 200, 400 and 600 µg mL^{-1}) in time periods of 24 h (a), 48 h (b), and 72 h (c) against MCF-7 cell line.

rGO-*g*-PDLA-*b*-P(NIPAAm-*rand*-AAc) at high concentration of nanocomposites (600 µg mL^{-1}) had biocompatible properties, thereby could be selected as an anticancer candidate for the nanomedicinal performances. Via further drug release and death of MCF-7 cells, the pH values increased, thereby the release content decreased parallel with the time elapsing (Figs. 10(a-c)). Based on DOX release and delivery strategies, the content of cell survivance was higher for the DOX-loaded rGO-*g*-PDLA-*b*-P(NIPAAm-*rand*-AAc) systems compared to the free DOX systems in the *in vitro* environments.

4. Conclusions

In summary, the rGO-based polymer brushes (rGO-*g*-PDLA-*b*-P(NIPAAm-*rand*-AAc)) were synthesized via surface initiated ROP and ATRP techniques. The modification was performed by polymerization of L,D-lactide from the surface of rGO and attaching the initiator to rGO-*g*-PDLA, the process was followed by the ATRP of NIPAAm and AAc through the grafting-from strategy. The control of drug release through the stimuli-responsive polymers on rGO nanosheets was investigated in response to the environmental temperature and pH. The drug deliverysystem of rGO-*g*-PDLA-*b*-P(NIPAAm-*rand*-AAc) demonstrated a very high DOX storage (98 %), attributing to the large two-dimensional plane of GO which provided large specific surface area and hydrogen bonding between the PNIPAAm, PAAc, and DOX. This work could provide a promising method for the surface functionalization of rGO for the drug delivery applications.

References

1. Portney NG, Ozkan M. Nano-oncology: drug delivery, imaging, and sensing. Analytical and Bioanalytical Chemistry. 2006;384(3):620-30.
2. Lomas H, Massignani M, Abdullah KA, Canton I, Lo Presti C, MacNeil S, et al. Non-cytotoxic polymer vesicles for rapid and efficient intracellular delivery. Faraday Discussions. 2008;139:143.
3. Gil E, Hudson S. Stimuli-reponsive polymers and their bioconjugates. Progress in Polymer Science. 2004;29(12):1173-222.
4. Zhang X-Z, Yang Y-Y, Chung T-S, Ma K-X. Preparation and Characterization of Fast Response Macroporous Poly(N-isopropylacrylamide) Hydrogels. Langmuir. 2001;17(20):6094-9.
5. Zareie HM, Volga Bulmus E, Gunning AP, Hoffman AS, Piskin E, Morris VJ. Investigation of a stimuli-responsive copolymer by atomic force microscopy. Polymer. 2000;41(18):6723-7.
6. Seo HI, Cheon YA, Chung BG. Graphene and thermo-responsive polymeric nanocomposites for therapeutic applications. Biomedical Engineering Letters. 2016;6(1):10-5.
7. Namvari M, Biswas CS, Galluzzi M, Wang Q, Du B, Stadler FJ. Reduced graphene oxide composites with water soluble copolymers having tailored lower critical solution temperatures and unique tube-like structure. Scientific reports. 2017;7:44508.
8. Schmaljohann D. Thermo- and pH-responsive polymers in drug delivery. Advanced Drug Delivery Reviews. 2006;58(15):1655-70.
9. Kanamala M, Wilson WR, Yang M, Palmer BD, Wu Z. Mechanisms and biomaterials in pH-responsive tumour targeted drug delivery: A review. Biomaterials. 2016;85:152-67.
10. de las Heras Alarcon C, Pennadam S, Alexander C. Stimuli Responsive Polymers for Biomedical Applications. ChemInform. 2005;36(26).
11. Jaymand M, Lotfi M, Lotfi R. Functional dendritic compounds: potential prospective candidates for dental restorative materials and in situ re-mineralization of human tooth enamel. RSC Advances. 2016;6(49):43127-46.
12. York A, Kirkland S, McCormick C. Advances in the synthesis of amphiphilic block copolymers via RAFT polymerization: Stimuli-responsive drug and gene delivery. Advanced Drug Delivery Reviews. 2008;60(9):1018-36.
13. Bains A, Wulff JE, Moffitt MG. Microfluidic synthesis of dye-loaded polycaprolactone- block -poly(ethylene oxide) nanoparticles: Insights into flow-directed loading and in vitro release for drug delivery. Journal of Colloid and Interface Science. 2016;475:136-48.
14. Huang J, Zhang H, Yu Y, Chen Y, Wang D, Zhang G, et al. Biodegradable self-assembled nanoparticles of poly (d,l-lactide-co-glycolide)/hyaluronic acid block copolymers for target delivery of docetaxel to breast cancer. Biomaterials. 2014;35(1):550-66.
15. Davaran S, Ghamkhari A, Alizadeh E, Massoumi B, Jaymand M. Novel dual stimuli-responsive ABC triblock copolymer: RAFT synthesis, "schizophrenic" micellization, and its performance as an anticancer drug delivery nanosystem. Journal of Colloid and Interface Science. 2017;488:282-93.
16. Yang M, Gong S. Immunosensor for the detection of cancer biomarker based on percolated graphene thin film. Chemical Communications. 2010;46(31):5796.
17. Rao CNR, Sood AK, Subrahmanyam KS, Govindaraj A. Graphene: The New Two-Dimensional Nanomaterial. Angewandte Chemie International Edition. 2009;48(42):7752-77.
18. Loh KP, Bao Q, Ang PK, Yang J. The chemistry of graphene. Journal of Materials Chemistry. 2010;20(12):2277.
19. Singh V, Joung D, Zhai L, Das S, Khondaker SI, Seal S. Graphene based materials: Past, present and future. Progress in Materials Science. 2011;56(8):1178-271.
20. Novoselov KS, Geim AK, Morozov SV, Jiang D, Katsnelson MI, Grigorieva IV, et al. Two-dimensional gas of massless Dirac fermions in graphene. Nature. 2005;438(7065):197-200.
21. Geim AK, Novoselov KS. The rise of graphene. Nature Materials. 2007;6(3):183-91.
22. Lee C, Wei X, Kysar JW, Hone J. Measurement of the Elastic Properties and Intrinsic Strength of Monolayer Graphene. Science. 2008;321(5887):385-8.
23. Li X, Li C, Zhu H, Wang K, Wei J, Li X, et al. Hybrid thin films of graphene nanowhiskers and amorphous carbon as transparent conductors. Chemical Communications. 2010;46(20):3502.
24. Mrlík M, Ilčíková M, Plachý T, Pavlínek V, Špitalský Z, Mosnáček J. Graphene oxide reduction during surface-initiated atom transfer radical polymerization of glycidyl methacrylate: Controlling electro-responsive properties. Chemical Engineering Journal. 2016;283:717-20.

25. Novoselov KS, Falʹko VI, Colombo L, Gellert PR, Schwab MG, Kim K. A roadmap for graphene. Nature. 2012;490(7419):192-200.

26. Bai H, Xu Y, Zhao L, Li C, Shi G. Non-covalent functionalization of graphene sheets by sulfonated polyaniline. Chemical Communications. 2009(13):1667.

27. Fang M, Wang K, Lu H, Yang Y, Nutt S. Covalent polymer functionalization of graphene nanosheets and mechanical properties of composites. Journal of Materials Chemistry. 2009;19(38):7098.

28. Lee SH, Dreyer DR, An J, Velamakanni A, Piner RD, Park S, et al. Polymer Brushes via Controlled, Surface-Initiated Atom Transfer Radical Polymerization (ATRP) from Graphene Oxide. Macromolecular Rapid Communications. 2009;31(3):281-8.

29. Ren L, Wang X, Guo S, Liu T. Functionalization of thermally reduced graphene by in situ atom transfer radical polymerization. Journal of Nanoparticle Research. 2011;13(12):6389-96.

30. Gonçalves G, Marques PAAP, Barros-Timmons A, Bdkin I, Singh MK, Emami N, et al. Graphene oxide modified with PMMA via ATRP as a reinforcement filler. Journal of Materials Chemistry. 2010;20(44):9927.

31. Yang Y, Wang J, Zhang J, Liu J, Yang X, Zhao H. Exfoliated Graphite Oxide Decorated by PDMAEMA Chains and Polymer Particles. Langmuir. 2009;25(19):11808-14.

32. Matyjaszewski K, Xia J. Atom Transfer Radical Polymerization. Chemical Reviews. 2001;101(9):2921-90.

33. Zhu S, Li J, Chen Y, Chen Z, Chen C, Li Y, et al. Grafting of graphene oxide with stimuli-responsive polymers by using ATRP for drug release. Journal of Nanoparticle Research. 2012;14(9).

34. Bastakoti BP, Guragain S, Nakashima K, Yamauchi Y. Stimuli-Induced Core-Corona Inversion of Micelle of Poly(acrylic acid)-block-Poly(N-isopropylacrylamide) and Its Application in Drug Delivery. Macromolecular Chemistry and Physics. 2014;216(3):287-91.

35. Massoumi B, Ghamkhari A, Agbolaghi S. Dual stimuli-responsive poly(succinyloxyethylmethacrylate-b-N-isopropylacrylamide) block copolymers as nanocarriers and respective application in doxorubicin delivery. International Journal of Polymeric Materials and Polymeric Biomaterials. 2017;67(2):101-9.

36. Sarvari R, Sattari S, Massoumi B, Agbolaghi S, Beygi-Khosrowshahi Y, Kahaie-Khosrowshahi A. Composite electrospun nanofibers of reduced graphene oxide grafted with poly(3-dodecylthiophene) and poly(3-thiophene ethanol) and blended with polycaprolactone. Journal of Biomaterials Science, Polymer Edition. 2017;28(15):1740-61.

37. Kimura K, Yanagida Y, Haruyama T, Kobatake E, Aizawa M. Gene expression in the electrically stimulated differentiation of PC12 cells. Journal of Biotechnology. 1998;63(1):55-65.

38. Yang J-H, Lin S-H, Lee Y-D. Preparation and characterization of poly(l-lactide)–graphene composites using the in situ ring-opening polymerization of PLLA with graphene as the initiator. Journal of Materials Chemistry. 2012;22(21):10805.

39. Song W, Zheng Z, Tang W, Wang X. A facile approach to covalently functionalized carbon nanotubes with biocompatible polymer. Polymer. 2007;48(13):3658-63.

40. Seligra PG, Nuevo F, Lamanna M, Famá L. Covalent grafting of carbon nanotubes to PLA in order to improve compatibility.

41. Liu M, Pu M, Ma H. Preparation, structure and thermal properties of polylactide/sepiolite nanocomposites with and without organic modifiers. Composites Science and Technology. 2012;72(13):1508-14.

42. Chen W, Yan L. Preparation of graphene by a low-temperature thermal reduction at atmosphere pressure. Nanoscale. 2010;2(4):559.

43. Sha J, Gao Y, Wu T, Chen X, Cordie T, Zhao H, et al. Biocompatible graphene nanosheets grafted with poly(2-hydroxyethyl methacrylate) brushes via surface-initiated ARGET ATRP. RSC Advances. 2016;6(42):35641-7.

44. Schilli CM, Zhang M, Rizzardo E, Thang SH, Chong YK, Edwards K, et al. A New Double-Responsive Block Copolymer Synthesized via RAFT Polymerization: Poly(N-isopropylacrylamide)-block-poly(acrylic acid). Macromolecules. 2004;37(21):7861-6.

45. Massoumi B, Sarvari R, Khanizadeh L, Agbolaghi S, Beygi-Khosrowshahi Y. pH-responsive nanosystems based on reduced graphene oxide grafted with polycaprolactone-block-poly(succinyloxyethylmethacrylate) for doxorubicin release. Journal of the Iranian Chemical Society. 2019;16(9):2031-43.

46. Ghamkhari A, Sarvari R, Ghorbani M, Hamishehkar H. Novel thermoresponsive star-liked nanomicelles for targeting of anticancer agent. European Polymer Journal. 2018;107:143-54.

47. Francis R, Jijil CP, Prabhu CA, Suresh CH. Synthesis of poly(N-isopropylacrylamide) copolymer containing anhydride and imide comonomers – A theoretical study on reversal of LCST. Polymer. 2007;48(22):6707-18.

48. You Y-Z, Oupický D. Synthesis of Temperature-Responsive Heterobifunctional Block Copolymers of Poly(ethylene glycol) and Poly(N-isopropylacrylamide). Biomacromolecules. 2007;8(1):98-105.

49. Guo Y, He W, Yang S, Zhao D, Li Z, Luan Y. Co-delivery of docetaxel and verapamil by reduction-sensitive PEG-PLGA-SS-DTX conjugate micelles to reverse the multi-drug resistance of breast cancer. Colloids and Surfaces B: Biointerfaces. 2017;151:119-27.

50. Song X, Zhu J-l, Wen Y, Zhao F, Zhang Z-X, Li J. Thermoresponsive supramolecular micellar drug delivery system based on star-linear pseudo-block polymer consisting of β-cyclodextrin-poly(N-isopropylacrylamide) and adamantyl-poly(ethylene glycol). Journal of Colloid and Interface Science. 2017;490:372-9.

51. Emamzadeh M, Desmaële D, Couvreur P, Pasparakis G. Dual controlled delivery of squalenoyl-gemcitabine and paclitaxel using thermo-responsive polymeric micelles for pancreatic cancer. Journal of Controlled Release. 2017;259:e90-e1.

52. Bigot J, Charleux B, Cooke G, Delattre Fo, Fournier D, Lyskawa Jl, et al. Tetrathiafulvalene End-Functionalized Poly(N-isopropylacrylamide): A New Class of Amphiphilic Polymer for the Creation of Multistimuli Responsive Micelles. Journal of the American Chemical Society. 2010;132(31):10796-801.

53. Ghorbani M, Hamishehkar H, Arsalani N, Entezami AA. Surface decoration of magnetic nanoparticles with folate-conjugated poly(N-isopropylacrylamide-co-itaconic acid): A facial synthesis of dual-responsive nanocarrier for targeted delivery of doxorubicin. International Journal of Polymeric Materials and Polymeric Biomaterials. 2016;65(13):683-94.

Composites Part B: Engineering. 2013;46:61-8.